

# Numerical Simulation and Experimental Study on Internal Depressurization Flow Characteristics of a Multi-layer Sleeve Regulating Valve

H. Z. Jin, K. M. Tang, X. F. Liu and C. Wang<sup>†</sup>

Faculty of Mechanical Engineering & Automation, Zhejiang Sci-Tech University, Hangzhou, Zhejiang, 310018, China

<sup>†</sup>Corresponding Author Email: [wangchao@zstu.edu.cn](mailto:wangchao@zstu.edu.cn)

(Received September 18, 2022; accepted December 26, 2022)

## ABSTRACT

The sleeve regulating valve is an important part of a pipeline system and is widely used in the fields of nuclear power and thermal power. In this study, a series of numerical and experimental studies are performed to understand the depressurized flow characteristics inside a new type of multi-layer sleeve regulating valve. In the calculations, the standard  $k$ - $\varepsilon$  turbulence model and the mixture model combined with the Zwart–Gerber–Belamri cavitation model are used to clarify the internal flow and cavitation characteristics in the regulating valve. With the new valve, the results show that when the valve is fully opened, the pressure drop at all levels of the valve is comparatively average (approximately 2–3 MPa for each level) and the fluid velocity in the sleeves at all levels is comparatively uniform at 90 m/s—which can prevent the valve from being eroded by highly changing fluid flow rates, and also offers ideal pressure reduction performance. To reduce the degree of cavitation, it is recommended to adjust the outlet pressure of the valve to 0.7 MPa.

**Keywords:** Regulating valve; Numerical simulations; Experimental verification; Flow characteristics; Cavitation.

## NOMENCLATURE

$3D$	three-dimensional	$R_B$	bubble radius
$G_k$	turbulence kinetic energy generation owing to mean velocity gradients	$\sigma_k$	turbulent Prandtl numbers for $k$
$G_b$	turbulence kinetic energy generation owing to buoyancy	$\sigma_\varepsilon$	turbulent Prandtl numbers for $\varepsilon$
$\alpha_{nuc}$	nucleation site volume fraction	$\rho$	mixture density
$F_{vap}$	evaporation coefficient	$\rho_v$	vapor density
$F_{cond}$	condensation coefficient	$\rho_l$	liquid density

## 1. INTRODUCTION

The regulating valve is a special kind of valve. During the operation of such a valve, the pressure, velocity, and temperature of the fluid medium change, and the flow field in the valve forms a complex flow with a high degree of turbulence. As an important type of regulating valve, the sleeve regulating valve is widely used in practice (Chen *et al.* 2018; Qian *et al.* 2020; Chen and Jin 2021; Ou *et al.* 2022). Its most important feature is that it has

good performance in adjusting the flow and pressure of the internal fluid medium, suppressing cavitation, and reducing vibration and noise under conditions of high pressure difference and high flow rate (Chen *et al.* 2017).

In the past few decades, several researchers have carried out numerical simulation studies on the internal flow characteristics of fluid in valves and other channels (Coşkun and Pehlivan 2021; Geng *et al.* 2021; Xavier and Ortiz 2021; Shahsavari *et al.* 2022). Ma *et al.* (2020) performed a transient

numerical simulation of the interior flow field in a ball valve for various flow speeds. Siddiqi *et al.* (2022) focused on the heat-transfer performance and pressure-drop characteristics of ZnO/DIW-based nanofluids (NFs) in horizontal mini tubes of different diameters. In a two-stage sleeve regulating valve, Yu *et al.* (2022) evaluated the effect of sleeve orifice ratio on flow performance and hydrodynamic noise. They also measured the flow-field pressure, velocity, turbulent kinetic energy, and sound pressure levels.

In addition to using computational fluid dynamics to carry out numerical simulations, many other scholars conducted corresponding experiments to verify the accuracy of numerical simulations (Asim *et al.* 2017; Cui *et al.* 2017; Yang *et al.* 2017; Derakhshan *et al.* 2019; Zawawi *et al.* 2022). Zhang *et al.* (2022) proposed a bionic valve core structure based on Bio-TRIZ, they explored the distribution of the pressure field, velocity field, and the cavitation field in a regulating valve, by experiment and simulation methods. In relief valves with an unconfined poppet, Yi *et al.* (2015) looked at the interactions between poppet vibration properties and cavitation. Zeng *et al.* (2015) conducted an experimental study on the internal flow characteristic of a control valve and the phenomena of sound mutation.

In sum, most researchers have used numerical simulations to determine the internal flow characteristics in regulating valves. There are few experimental studies that confirm the accuracy of these numerical simulations. Additionally, the flow characteristics of the multi-layer sleeve regulating valve used in this paper are less investigated than those in the current literature, which focus primarily on the flow characteristics of the single-layer regulating valve. It is difficult to predict and prevent cavitation failure under high-risk operating conditions owing to the lack of studies on cavitation failure in multi-layer sleeve regulating valves, presenting a significant challenge for the engineering application of the regulating valve. This work examines the internal flow characteristics of a multi-layer sleeve regulating valve as used in nuclear power. A novel experimental investigation has been conducted to determine the internal flow characteristics within the valve flow channel. The cavitation failure in a multi-layer sleeve regulating valve at different opening degrees is also researched.

## 2. APPLICATION BACKGROUND AND EXPERIMENT SET-UP

### 2.1 Application Background

The flow chart of the main water supply system of a nuclear power plant is shown in Fig. 1. It is composed of three feed pumps, two rows of high-pressure heaters, and related pipes and valves. Its main function is to provide the steam generators with water under a certain pressure and temperature. Water, provided by a CPS-21F water-supply

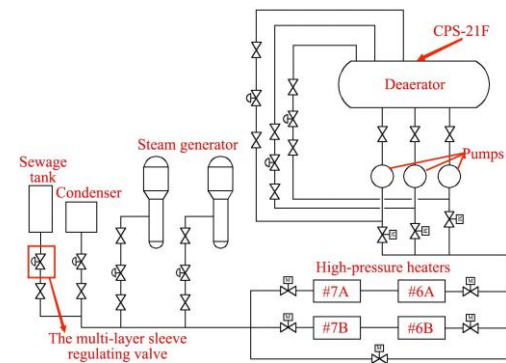


**Fig. 1. Flow chart of the main water supply system of a nuclear power plant.**

controller, enters the de-aerator to remove oxygen and other gases, it then passes through three pumps to be pressurized. After being pressurized, it flows through two rows of high-pressure heaters (#6A, #7A, #6B, and #7B) to be heated. Finally, it enters the steam generator through the main feed-water flow regulating valve. There is a connection door between the start feed water and the main feed water. The main feed water enters the steam generator via the feed-water pipeline. A pipeline is led from the main water supply pipe to the condenser and the sewage tank which is used to start the initial flushing of the main water supply system, this pipeline section is called the long cycle.

The multi-layer sleeve regulating valve as used in a nuclear power main water supply system is located between the long cycle and the sewage tank (this position is shown in the red box in Fig. 1). Its main function is to regulate the pressure of water flowing into the sewage tank. Considering that the main water supply system of a nuclear power is at high temperature and high differential pressure, cavitation failure and other problems with the regulating valve will inevitably occur. Therefore, it is important to understand the internal flow characteristics of the multi-layer sleeve regulating valve; its application conditions are listed in Table 1.

**Table 1 Working condition of the valve.**

Material	Water-Liquid	Water-Vapor
Temperature/ K	394.15	
Density/ $\text{kg}\cdot\text{m}^{-3}$	942.2987	1.1557
Viscosity/ $\text{kg}\cdot\text{s}\cdot\text{m}^{-2}$	$2.34515\text{e}^{-5}$	$1.32167\text{e}^{-6}$
Vaporization pressure/ MPa	0.205	
Inlet pressure/ MPa	9.4	
Outlet pressure/ MPa	0.11	

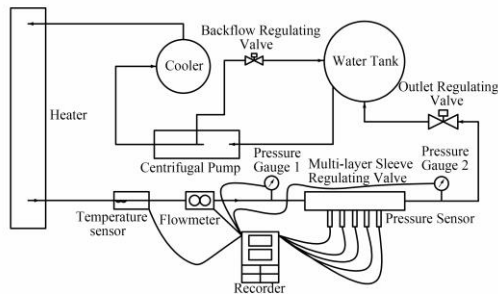


**Fig. 2.** Flow chart of the experiment.

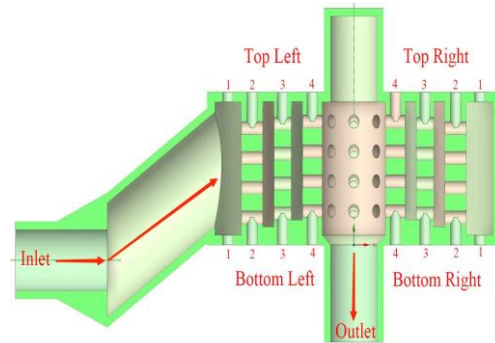
## 2.2 Experimental Preparations

Figure 2 shows the design flow chart of the experimental device for the internal depressurized flow characteristics of the multi-layer sleeve regulating valve. The entire device process contains a power device, a constant temperature device, a control device, a display device, and the multi-layer sleeve regulating valve, forming a circulating water channel connected by the pipeline.

The water at the outlet of the centrifugal pump flows in two directions, one route flows back to the water tank through the backflow regulating valve, and the other passes through the cooler and heater, runs through the temperature sensor and flowmeter, and subsequently enters the valve before eventually returning to the water tank through the outlet regulating valve. Pressure values at selected measuring points inside the multi-layer sleeve regulating valve are measured by a pressure sensor. The pressure sensor is used to monitor the pressure signals at different positions of the flow channel, and pressure gauges 1 and 2 are used to monitor and adjust the pressure at the inlet and outlet of the multi-layer sleeve regulating valve to ensure stable operation. A recorder transforms the measurement signals in the experiment into real-time data. The functions of the cooler and the heater are to prevent the centrifugal pump from over running, which will cause the water temperature to rise and adversely affect the experimental measurement results.

The pressure sensor used in this experiment was a digital-display pressure sensor, which can display measured pressure in real-time. The range of the sensor is 0–0.60 MPa, and the measurement accuracy is  $\pm 0.1\%$ , which meets the requirements of the experiment of the internal depressurized flow characteristics of the multi-layer sleeve regulating valve.

Owing to the complex structure and extreme application conditions of the multi-layer sleeve regulating valve, the valve model used under actual working conditions is costly and hard to obtain. Because of the large number and dense distribution of small holes at the valve seat, the experimental multi-layer sleeve model outlet flow channels were



**Fig. 3.** The 3D-printed multi-layer sleeve regulating valve model.

simplified to meet the requirements of the experiment, as shown at Fig. 3.

The method of 3D printing was used, with white resin, to form the experimental model of the valve.

The white resin material used in this process has the characteristics of high strength, good toughness, and easy processing. It is widely used in experimental research for closed internal flow channels, or parts that cannot be processed by lathes, or components which are processed with high precision, such as bellows and centrifugal pump impellers.

To clarify the depressurization capability of each level of sleeve inside the multi-layer sleeve regulating valve, four data collection points were designed at each level of the sleeve along the flow direction of water (as shown in Fig. 3).

The valve used in this experiment can ensure the accuracy of the internal position of the flow field measured by the sensor. The resin material does not affect the measured value of pressure. This meets the requirements of strength and hardness in this experiment. However, the resin is prone to brittle fracture, and the installation process cannot be subjected to large shear stress. If metal processing is used to make a regulating valve, it will seriously affect the sealing performance of the internal flow channel of the valve, and it will also cause deviation of the internal flow channel size of the valve core, which will affect the experimental measurement results.

## 2.3 Experiment Process

The flow chart of the experimental set-up is shown in Fig. 4. First, the backflow regulating valve is closed while the inlet regulating valve and outlet regulating valve of the test section are fully open. Following this, pressure gauge 2 (see Fig. 4) is kept at 0 MPa, which represents the outlet pressure of the valve. Finally, the inlet regulating valve is gradually closed, so that the valve inlet pressure, shown by pressure gauge 1, is maintained variously at 0.45

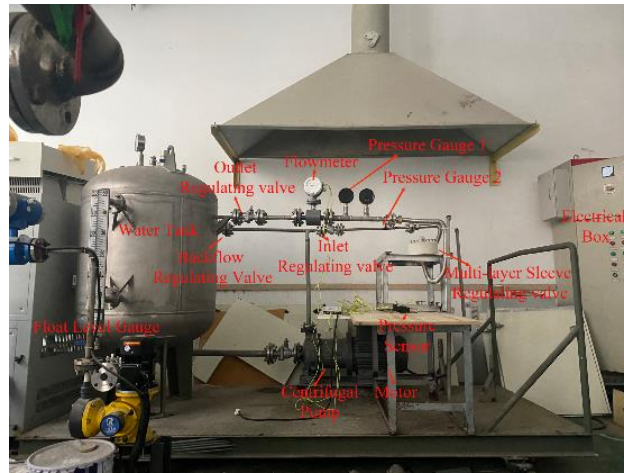


**Fig. 4.** Flow chart of the experimental device



**Fig. 5.** Installation method of the multi-layer sleeve regulating valve.

MPa, 0.40 MPa, and 0.35 MPa, respectively. The whole experiment was carried out at room temperature, and water was used as the experimental fluid. Figure 5 shows the installation method of the multi-layer sleeve regulating valve.

### 3. NUMERICAL METHODS

#### 3.1 Mesh and Geometry Model

The multi-layer sleeve regulating valve is a new type of regulating valve; designed by using two layers of orifice sleeves rather the traditional single-layer sleeve used in conventional regulating valves. The overall structure of the valve is shown in Fig. 6. It is mainly composed of the valve body, valve seat, multi-layer sleeve components, valve core, valve stem, valve cover, sealing device, and other smaller components. Figure 7 shows the multi-layer sleeve component of the valve core. The core is made of three layers of sleeves with openings; each sleeve layer is evenly distributed with 32 cylindrical orifices. When the fluid medium flows into the sleeve regulating valve, the unopened parts of the multi-layer sleeves block the movement of the fluid and reduces the pressure of the fluid medium. The

depressurized fluid then flows from the cylindrical orifices of the sleeve into the next sleeve for subsequent depressurization.

ANSYS/FLUENT meshing was used to create the computational mesh domains of the multi-layer sleeve regulating valve (Fig. 8). When flowing through the multi-layer sleeve, the fluid medium passes through an inlet and outlet pipe with a length of 500 mm, so that the flow is fully developed, and the flow rate is steady. The meshing strategy used in

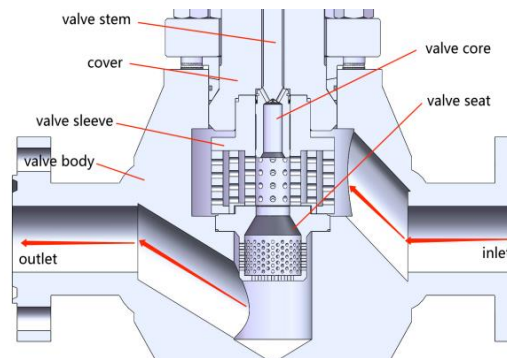


**Fig. 6.** Overall structure of the valve.

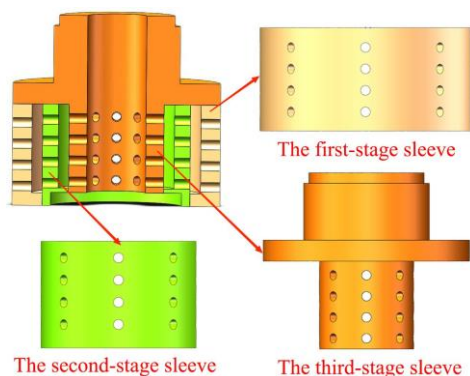


**Fig. 7.** Multi-layer sleeve component.

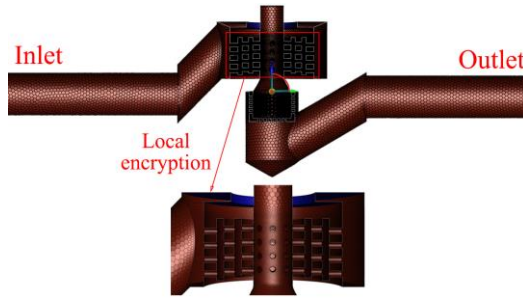


Fig. 8. Mesh of the multi-layer sleeve valve.

Table 2 Mesh specification.

Mesh	Number of cells	Outlet mass flow rate (kg/s)
M1	1.47 million	97.0267
M2	2.02 million	99.6294
M3	2.85 million	101.4456
M4	3.44 million	102.9874
M5	4.17 million	103.2547

this work incorporated the use of unstructured Poly-Hexcore meshes; the interior of the model was filled with regular hexahedrons. To ensure that the internal throttling passage of the multi-layer sleeve regulating valve had sufficient mesh nodes, the valve was divided in an encrypted way. The total number of cells after encryption was 3.44 million.

In ANSYS, the lattice faces should be meshed using the appropriate elements. In addition, the mesh quality should be thoroughly verified to avoid unrealistic meshes with excess distortion and size changes (Alqahtani *et al.* 2023). To determine the appropriate number of mesh cells, test meshes of 1.47 million, 2.02 million, 2.85 million, 3.44 million, and 4.17 million grids were selected for mesh independence verification. The valve outlet mass flow rates, open 100%, corresponding to the different mesh sizes are listed in Table 2. With increasing cell number, the outlet flow rate gradually tends to a stable value, and there is no remarkable difference between the calculated results for different mesh sizes; for M4 and M5 deviation is minimal. After comprehensively considering the factors of calculation efficiency and calculation accuracy, the mesh model of 3.44 million cells was selected to calculate the internal flow characteristics of the multi-layer sleeve regulating valve.

### 3.2 Turbulence Model

Because the actual flow inside the multi-sleeve regulating valve is extremely sophisticated, we chose the standard  $k-\varepsilon$  turbulence model to model turbulence, in that it is beneficial to deal with

turbulence for Reynolds numbers higher than 107 (Qiu *et al.* 2019). The turbulent kinetic energy  $k$  and its dissipation rate  $\varepsilon$  are respectively given by the following transport equations:

$$\frac{\partial}{\partial t}(\rho k) + \frac{\partial}{\partial x_i}(\rho k u_i) = \frac{\partial}{\partial x_j} \left[ \left( \mu + \frac{\mu_t}{\sigma_k} \right) \frac{\partial k}{\partial x_j} \right] + G_k + G_b - \rho \varepsilon + S_k \quad (1)$$

$$\frac{\partial}{\partial t}(\rho \varepsilon) + \frac{\partial}{\partial x_i}(\rho \varepsilon u_i) = \frac{\partial}{\partial x_j} \left[ \left( \mu + \frac{\mu_t}{\sigma_\varepsilon} \right) \frac{\partial \varepsilon}{\partial x_j} \right] + C_{1\varepsilon} \frac{\varepsilon}{k} (G_k + C_{3\varepsilon} G_b) - C_{2\varepsilon} \rho \frac{\varepsilon^2}{k} + S_\varepsilon \quad (2)$$

where  $u_i$  represents the velocity components,  $G_k$  represents turbulence kinetic energy generation owing to mean velocity gradients,  $G_b$  represents turbulence kinetic energy generation caused by buoyancy,  $C_{1\varepsilon}$ ,  $C_{2\varepsilon}$ , and  $C_{3\varepsilon}$  are constants,  $\sigma_k$  and  $\sigma_\varepsilon$  are the turbulent Prandtl numbers for  $k$  and  $\varepsilon$ , respectively, and  $S_k$  and  $S_\varepsilon$  are source terms defined by the user.

The turbulent viscosity  $\mu_t$  is computed using  $k$  and  $\varepsilon$  as follows:

$$\mu_t = \rho C_\mu \frac{k^2}{\varepsilon} \quad (3)$$

where  $C_\mu$  is a constant,  $C_{1\varepsilon} = 1.44$ ,  $C_{2\varepsilon} = 1.92$ ,  $C_\mu = 0.09$ ,  $\sigma_k = 1.0$ , and  $\sigma_\varepsilon = 1.3$ .

### 3.3 Multiphase Model

The mixture multiphase flow model is used in this research. The fluid medium is regarded as a two-phase uniform flow, in which liquid water is the main phase and water vapor is the secondary phase. The mixture medium is regarded as a 'single-phase' flow (Echouchene *et al.* 2011). The continuity equation and momentum equation are as follows (Yuan *et al.* 2001).

Continuity equation:

$$\frac{\partial \rho}{\partial t} + \frac{\partial \rho u_j}{\partial x_j} = 0 \quad (4)$$

Momentum equation:

$$\frac{\partial \rho u_i}{\partial t} + \frac{\partial \rho u_i u_j}{\partial x_j} = - \frac{\partial p}{\partial x_i} + \left[ (\mu + \mu_t) \left( \frac{\partial u_i}{\partial x_j} + \frac{\partial u_j}{\partial x_i} - \frac{2}{3} \delta_{ij} \frac{\partial u_k}{\partial x_k} \right) \right] \quad (5)$$

$$\rho = \alpha \rho_v + (1 - \alpha) \rho_l \quad (6)$$

$$\mu = \alpha\mu_v + (1 - \alpha)\mu_l \tag{7}$$

$$\alpha = f \frac{\rho}{\rho_v} \tag{8}$$

where  $u_i$  and  $u_j$  represent instantaneous velocity in the  $i$  and  $j$  directions,  $\rho_v$  and  $\rho_l$  represent the density of vapor and liquid, respectively,  $\mu$  is the mixture viscosity,  $\mu_v$  is the gas phase viscosity,  $\mu_l$  is the liquid phase viscosity,  $\alpha$  is the gas-phase volume fraction,  $f$  is the vapor mass fraction when  $i=j$ , and we use the Kronecker symbol  $\delta_{ij} = 1$ .

### 3.4 Cavitation Model

The bubble volume fraction, evaporation coefficient, and condensation coefficient are the three key parameters of the Zwart–Gerber–Belamri cavitation model. This model examines the gas core density in the evaporation term. It neglects bubble surface tension, the second derivative term, and assumes that all bubbles in the system are the same size. This model gives satisfactory performance and numerical stability and is adopted in this study (Xu *et al.* 2021).

The governing equations are given by:

$$\frac{\partial}{\partial t}(f_v \rho) + \nabla \cdot (f_v \rho \vec{V}_v) = \nabla \cdot (\Gamma \nabla f_v) + R_e - R_c \tag{9}$$

where  $f_v$  is vapor mass fraction,  $\vec{V}_v$  is vapor-phase velocity,  $R_e$  is evaporation rate,  $R_c$  is condensation rate, and  $\Gamma$  is the diffusion coefficient. The model evaporation and condensation rates are as follows:

When  $P \leq P_v$ ,

$$R_c = F_{vap} \frac{3\alpha_{nuc}(1 - \alpha_v)\rho_v}{RB} \left( \frac{2(P_v - P)}{3 P_l} \right)^{1/2} \tag{10}$$

When  $P \geq P_v$ ,

$$R_e = F_{cond} \frac{3\alpha_v \rho_v}{RB} \left( \frac{2(P - P_v)}{3 \rho_l} \right)^{1/2} \tag{11}$$

$$RB = \left( \frac{\alpha}{1 - \alpha} \frac{3}{4\pi} \frac{1}{n} \right)^{1/3} \tag{12}$$

$$P_v = P_{sat} + \frac{1}{2}(0.39\rho k) \tag{13}$$

where  $P_{sat}$  is the saturated vapor pressure,  $P_v$  is the corrected saturated vapor pressure,  $\alpha_{nuc} = 5 \times 10^4$ ,  $F_{vap} = 50$ , and  $F_{cond} = 0.01$ .

**Table 3 Key numerical calculation methods set in FLUENT.**

Parameter	Condition
Valve opening	25%, 50%, 75%, 100%
Inlet pressure	9.4 MPa
Outlet pressure	0.11 MPa
Temperature	394.15 K
Vaporization pressure	0.205 MPa
Turbulence model	Standard $k-\epsilon$
Multiphase model	Mixture
Cavitation model	Zwart–Gerber–Belamri
Wall	No slip
Pressure–velocity coupling	SIMPLE

### 3.5 Simulation Settings

In this study, ANSYS FLUENT 2021 was used to simulate the internal flow characteristic of the regulating valve. The incompressible two-phase flow with liquid water as the main phase and water vapor as the secondary phase were set as the fluid medium. Pressure inlet and outlet values were respectively adopted for the inlet and outlet boundary conditions. The inlet pressure was set at 9.4 MPa and the outlet pressure to 0.11 MPa. The full boundary conditions are listed in Table 3.

## 4. RESULTS AND DISCUSSION

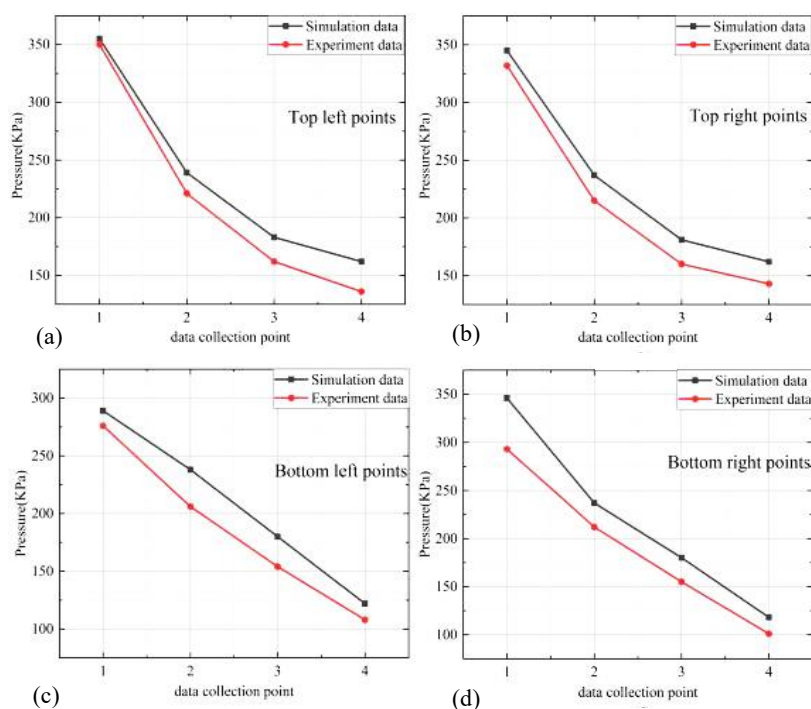
### 4.1 Experiment Results

Table 4 lists the pressure values of the numerical simulations at each of the data collection points. The pressure values of each of the data collection points of the multi-layer sleeve regulating valve obtained by the experiment are listed in Table 5.

The curves drawn from the experimental and simulated pressure values of each of the data collection points at different inlet pressure are shown in Figs. 9–11. The depressurized flow characteristics of the experiments and numerical simulations under the three working conditions are basically the same, and the pressure values of the sleeves at all levels generally decrease linearly and uniformly. The difference is that the pressure value curve of the numerical simulation is higher than that of the experimental measurement. The reason for this is that supplementary flow resistance is generated during the experimental installation of the multi-layer sleeve regulating valve, and the inner flow channel of the 3D printed valve was of a relatively rough finish. The rough internal surface imparts resistance to the flow and thus causes energy loss of the fluid. Furthermore, the pressure calculated by the

**Table 4 Simulation results of data collection points at different inlet pressures.**

450–0 KPa				
Location Direction	Point 1	Point 2	Point 3	Point 4
Top left	355 KPa	239 KPa	183 KPa	162 KPa
Bottom left	289 KPa	238 KPa	180 KPa	122 KPa
Top right	345 KPa	237 KPa	181 KPa	162 KPa
Bottom right	346 KPa	237 KPa	180 KPa	118 KPa
400–0 KPa				
Location Direction	Point 1	Point 2	Point 3	Point 4
Top left	315 KPa	213 KPa	163 KPa	145 KPa
Bottom left	257 KPa	212 KPa	161 KPa	109 KPa
Top right	307 KPa	212 KPa	162 KPa	144 KPa
Bottom right	308 KPa	211 KPa	161 KPa	106 KPa
350–0 KPa				
Location Direction	Point 1	Point 2	Point 3	Point 4
Top left	276 KPa	187 KPa	143 KPa	127 KPa
Bottom left	225 KPa	186 KPa	141 KPa	96 KPa
Top right	269 KPa	185 KPa	142 KPa	127 KPa
Bottom right	270 KPa	185 KPa	141 KPa	93 KPa



**Fig. 9. Comparison of experimental and simulated pressure values at 450–0 KPa. (a) Top left points, (b) Top right points, (c) Bottom left points, and (d) Bottom right points.**

**Table 5** Experimental results of data collection points at different inlet pressures.

450–0 KPa				
Location Direction	Point 1	Point 2	Point 3	Point 4
Top left	350 KPa	221 KPa	162 KPa	136 KPa
Bottom left	276 KPa	206 KPa	154 KPa	108 KPa
Top right	332 KPa	215 KPa	160 KPa	143 KPa
Bottom right	293 KPa	212 KPa	155 KPa	101 KPa
400–0 KPa				
Location Direction	Point 1	Point 2	Point 3	Point 4
Top left	300 KPa	191 KPa	146 KPa	122 KPa
Bottom left	239 KPa	191 KPa	146 KPa	88 KPa
Top right	287 KPa	184 KPa	146 KPa	120 KPa
Bottom right	272 KPa	190 KPa	146 KPa	87 KPa
350–0 KPa				
Location Direction	Point 1	Point 2	Point 3	Point 4
Top left	268 KPa	165 KPa	122 KPa	113 KPa
Bottom left	212 KPa	164 KPa	125 KPa	81 KPa
Top right	258 KPa	168 KPa	128 KPa	113 KPa
Bottom right	263 KPa	171 KPa	128 KPa	76 KPa

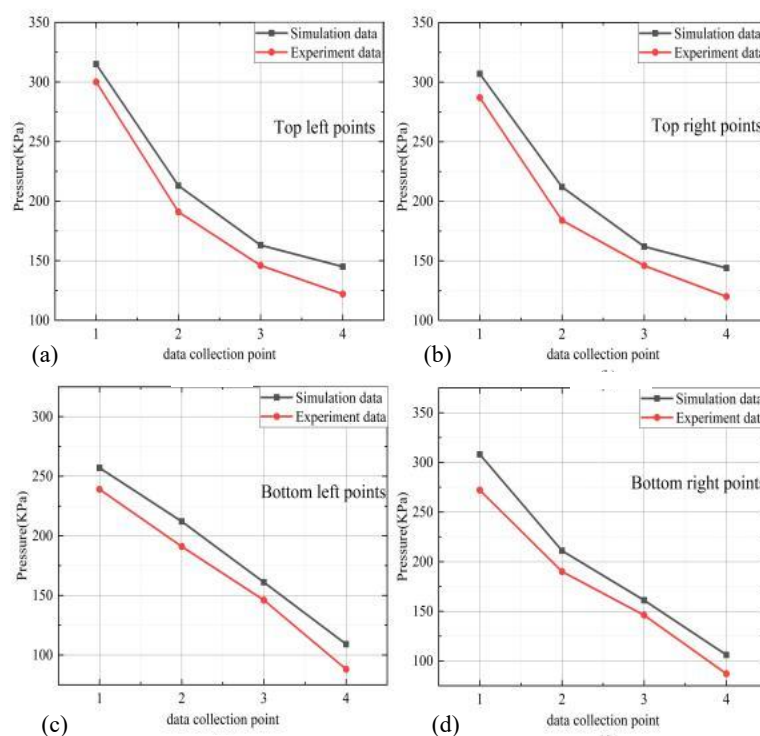


**Fig. 10.** Comparison of experimental and simulated pressure values at 400–0 KPa. (a) Top left points, (b) Top right points, (c) Bottom left points, and (d) Bottom right points.

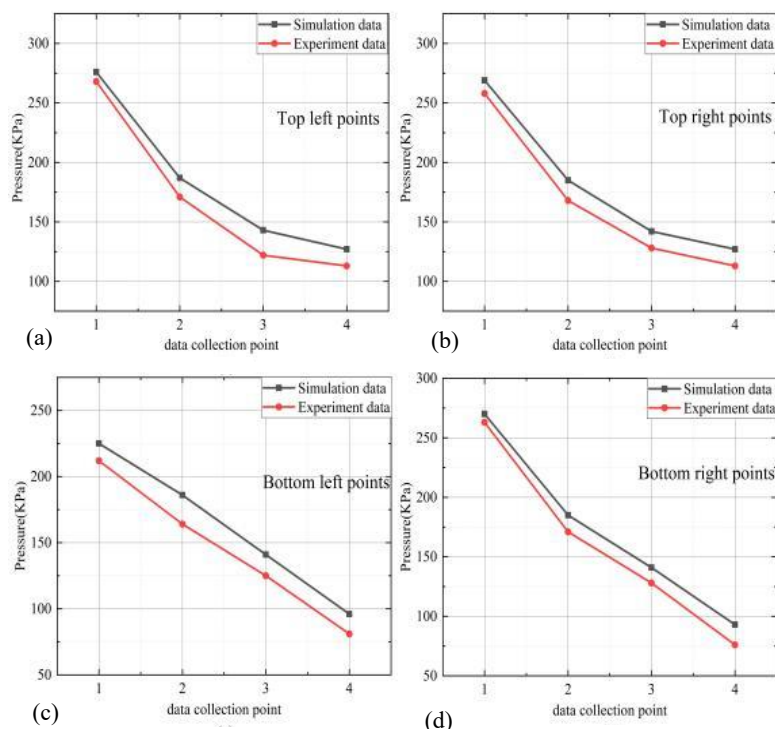


**Fig. 11.** Comparison of experimental and simulated pressure values at 350–0 KPa. (a) Top left points, (b) Top right points, (c) Bottom left points, and (d) Bottom right points.

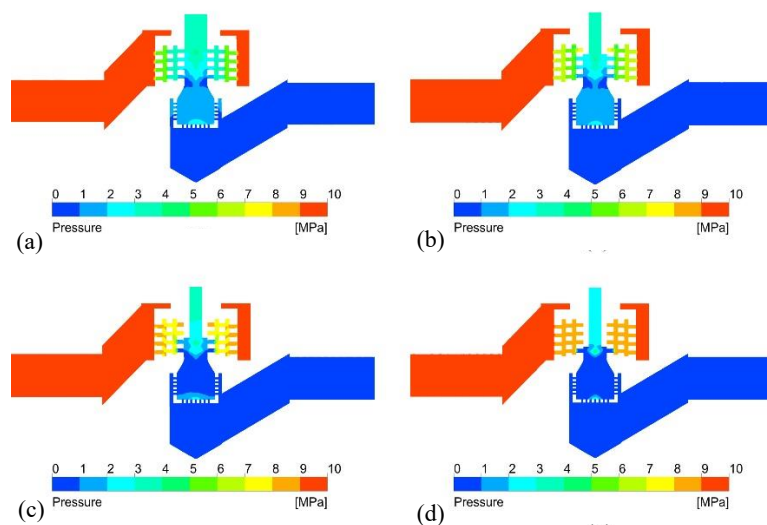


**Fig. 12.** Internal fluid pressure distribution of the valve under different opening conditions. (a) 100% open, (b) 75% open, (c) 50% open, and (d) 25% open.

numerical simulation was under ideal conditions, which were different from those of the actual conditions. The variation law of the pressure values of each of the data collection points, measured by numerical simulation and the experiment, show the accuracy of the numerical model adopted in this paper, and that the variation law of the internal depressurization flow characteristics of the multi-layer sleeve regulating valve obtained by the

numerical simulation is correct.

#### 4.2. Fluid Pressure Distribution in the Valve

Figure 12 shows the internal fluid pressure distribution of the multi-layer sleeve regulating valve under different opening conditions at 394.15 K. Overall, despite the complicated internal flow channel structure of the valve, the fluid pressure at

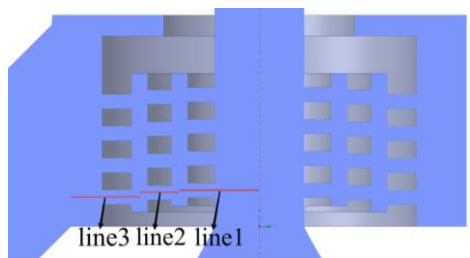


**Fig. 13. Simulation data acquisition positions.**

the inlet is always stable at 9.4 MPa, while the fluid pressure at the outlet is always kept at 0.11 MPa.

To analyze the internal flow characteristics of the sleeve regulating valve, the central axes of the orifices at the bottom of the sleeve at all levels are selected to acquire simulation results, as shown in Fig. 13.

Overall, the pressure-change trends of the fluid inside the regulating valve remained basically the same even when changing the opening conditions (Fig. 14). After the fluid passes through the 500 mm inlet flow channel, its pressure becomes stable. The pressure of the fluid flowing into the multi-layer sleeve component of the valve is maintained at approximately 9.3 MPa before flowing into each of the stage sleeves to be depressurized. There is a buffer section between each of the stage sleeves. When the fluid flows into the buffer section, it is fully mixed before flowing into the next sleeve stage prior to further depressurizing. After the fluid flows through the multi-layer sleeve components, it then flows into the middle valve core with larger spaces, so the pressure of the fluid flowing from the third-stage sleeve to the middle valve core rises to a certain extent. The fluid then flows into the valve seat and finally flows out of the multi-layer sleeve regulating valve. There is also a pressure drop of the fluid at the valve seat.

The pressure of the fluid in each level of the sleeves has obvious differences as the opening degree of the

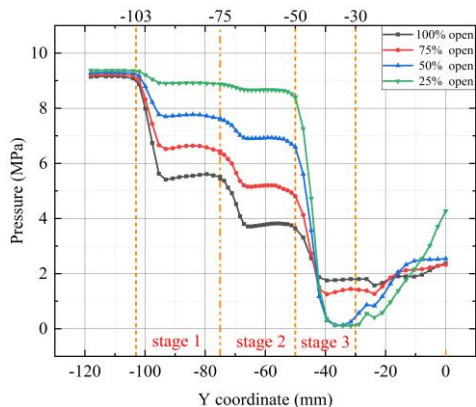


**Fig. 14. Internal depressurization flow characteristics of multi-layer sleeve regulating valve under different opening degrees.**

regulating valve changes. When the valve is fully opened, there is little difference in the depressurization capability of the sleeves at all levels. The first-stage sleeve bears a relatively larger pressure drop (approximately 3.5 MPa), while the second- and third-stage sleeves have similar pressure-relief capabilities (approximately 2 MPa). As the opening of the valve is reduced to 75%, the fluid pressure drop borne by the first-stage sleeve is also reduced to approximately 2.8 MPa, the second-stage sleeve provides a pressure drop of approximately 2 MPa, and the fluid pressure drop borne by the third-stage sleeve increases to 3.2 MPa. As the valve opening is further reduced to 50%, the fluid pressure drop borne by the first- and second-stage sleeves is reduced ulteriorly, reaching 1.7 MPa and 1.1 MPa, respectively, while the fluid pressure drop borne by the third-stage sleeve sharply increases to 6 MPa, which undertakes most of the depressurization effect of the multi-layer sleeve regulating valve. As the valve opening is reduced to 25%, the third-stage sleeve becomes the main depressurizing part of the multi-layer sleeve component, the fluid pressure drop reaches approximately 8 MPa, while the fluid pressure drop borne by the first and second-stage sleeves is merely 0.5 MPa.

In general, the multi-layer sleeve component of the valve can complete the depressurization of the internal fluid at various opening amounts. When the valve is fully opened, the pressure drop of the fluid in the sleeves at all levels of the valve is relatively stable (2–3 MPa pressure drop for each level); this offers the most ideal pressure reduction performance.

### 4.3 Fluid Velocity Distribution in the Valve

Like the fluid pressure inside the valve, the velocity distribution of the fluid inside the multi-layer sleeve regulating valve at different opening degrees is also obtained (Fig. 15). The fluid velocity at the inlet and the outlet remains stable at 10 m/s under different opening degrees. When the fluid passes through the multi-layer sleeve component, the fluid velocity changes significantly owing to the throttling effect of the small orifices in the sleeve.

Like the analysis of the fluid pressure in the multi-layer sleeve regulating valve, the same three axis lines are selected to analyze the fluid velocity in the regulating valve. Figure 16 shows the internal fluid velocity variation in the multi-layer sleeve regulating valve.

The fluid velocity variation trend inside the regulating valve is approximately the same when the opening degree changes. After the fluid passes through the 500 mm inlet flow channel, its velocity remains stable. When the fluid flows into the multi-layer sleeve component in the valve, the fluid velocity rises sharply. Then the fluid flows into the buffer region with larger flowing spaces, where the

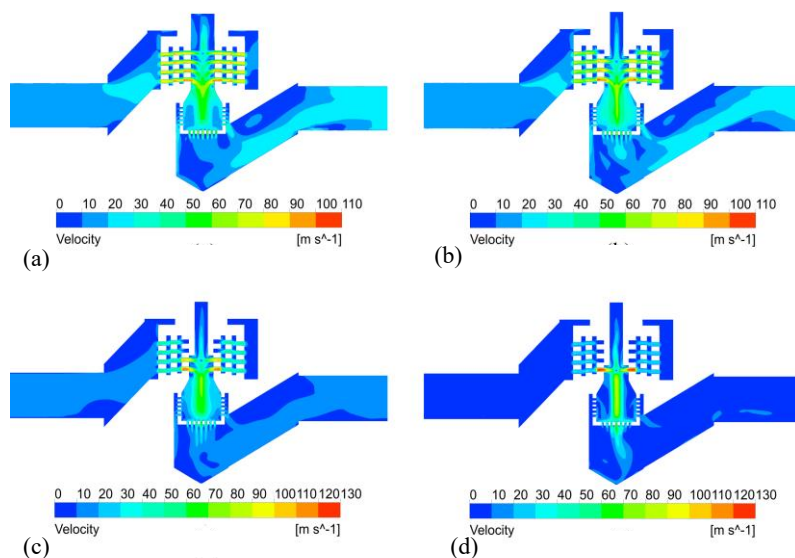


**Fig. 15.** Internal fluid velocity distribution of the valve under different opening degrees. (a) 100% open, (b) 75% open, (c) 50% open, and (d) 25% open.

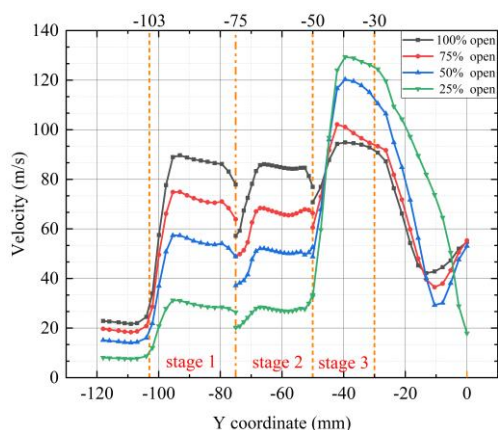


**Fig. 16.** Internal fluid velocity variation of multi-layer sleeve regulating valve under different opening.

fluid flow rate drops to a stable level. It then continues to flow into the next stage sleeve. When the fluid flows through the multi-layer sleeve component, it enters the middle valve core (which has a relatively larger volume), so that the velocity of the fluid flowing from the third-stage sleeve to the middle valve core is reduced.

There are differences in the velocity of the fluid inside the valve at different openings. When the valve is fully open, the fluid velocity inside the sleeves at all levels changes somewhat unpredictably. The first-stage sleeve accelerates the fluid velocity from 25 m/s to 77 m/s, the second-stage sleeve accelerates the fluid velocity from 56 m/s to 76 m/s, and the third-stage sleeve increases the fluid velocity from 70 m/s to 90 m/s. The reason

for the decrease in fluid velocity is the presence of buffers among the sleeves at all levels. As the valve opening decreases, the fluid velocity in the first and second stage sleeves decreases accordingly. For example, when the valve opening decreases from 100% to 75%, to 50% and to 25%, the maximum fluid velocity in the first-stage sleeve drops from 90 m/s to 75 m/s, then 57 m/s, and finally 31 m/s, respectively. However, as the valve opening decreases, the fluid velocity inside the third-stage sleeve increases. The maximum velocity of the fluid in the third-stage sleeve gradually increased from 94 m/s to 102 m/s, 120 m/s, and 129 m/s. In addition, there is also a certain velocity change across the valve seat.

In general, the fluid velocity changes in the sleeves at all levels of the valve core are relatively uniform at 90 m/s when the valve is fully opened; this helps avoid erosion of the valve by fluid in a state of highly fluctuating flow rates.

#### 4.4 Cavitation in the Valve

By synthesizing the internal fluid velocity and pressure distribution in the multi-layer sleeve regulating valve, it can be seen that owing to the throttling effect of the small hole in the sleeve component, the fluid velocity at the third-stage sleeve is the highest, and the pressure is extremely low.

The entire main water supply system is at high temperature which leads to a high saturated vapor pressure of the fluid. When the fluid pressure is lower than its saturated vapor pressure, the fluid converts from liquid to vapor, causing cavitation inside the valve. Figure 17 shows the vapor

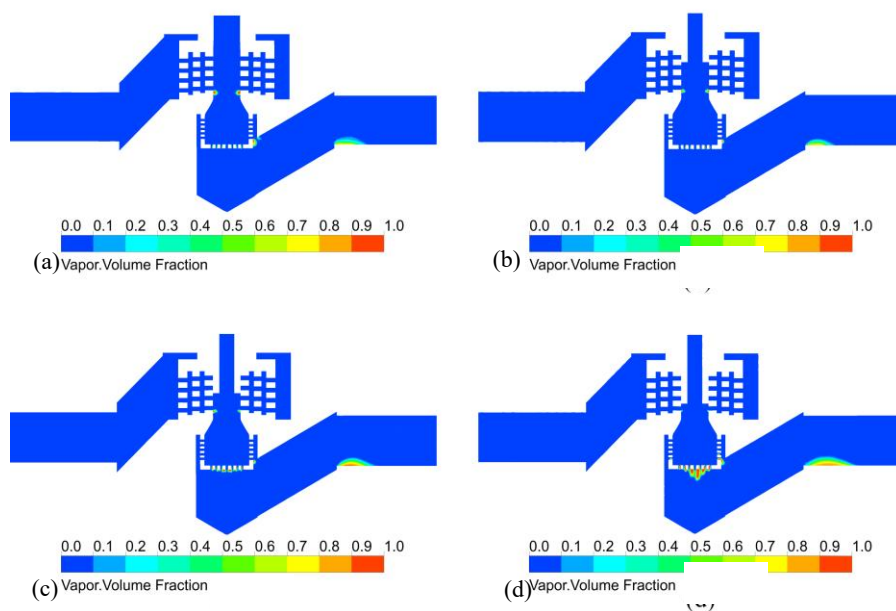


**Fig. 17. Internal vapor distribution of the valve under different opening degrees. (a) 100% open, (b) 75% open, (c) 50% open, and (d) 25% open.**

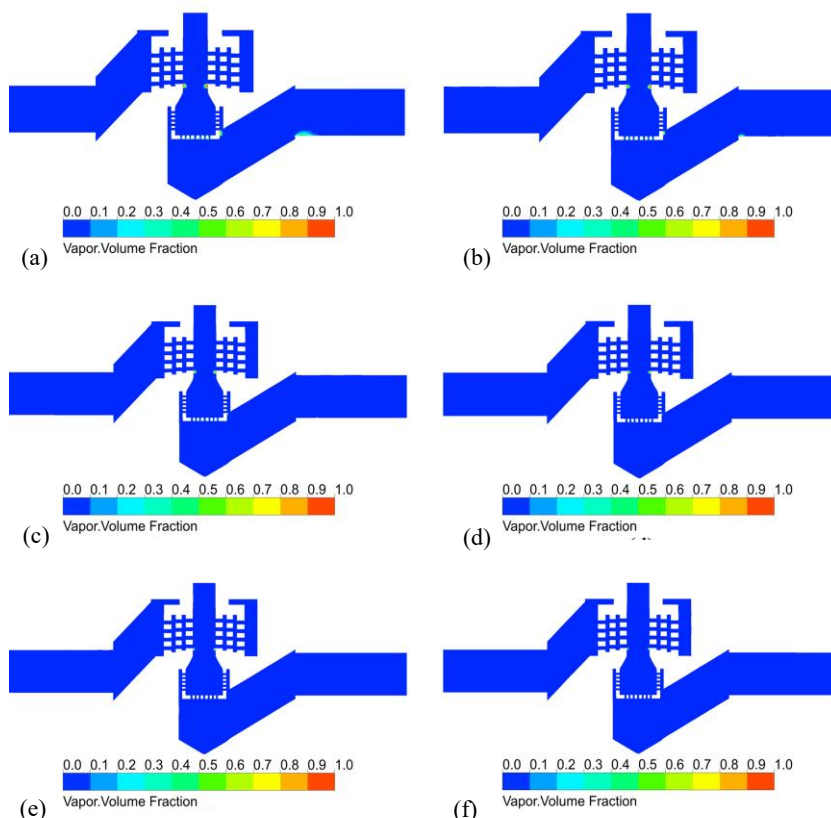


**Fig. 18. Internal vapor distribution of the valve under different outlet valve pressures. (a) 0.205 MPa, (b) 0.31 MPa, (c) 0.40 MPa, (d) 0.50 MPa, (e) 0.60 MPa, and (f) 0.70 MPa.**

distribution inside the valve under different opening degrees. There are approximately three positions

where the vapor appears inside the valve under different opening degrees. The first one is at the

small hole near the wall of the third-stage sleeve, the second one appears at the small holes at the valve seat, and the third one is located at the turning point of the outlet flow channel.

The degree of cavitation at each position is different under different opening degrees. When the multi-layer sleeve regulating valve is fully open, the degree of cavitation at the third-stage sleeve is most severe, and the cavitation area of the small hole at the valve seat is large but light. With the decrease of the valve opening, the cavitation degree at the third-stage sleeve reduces correspondingly, however, the decrease is not large, but the cavitation degree of the small holes at the valve seat increases correspondingly; the increase is relatively large. In addition, the change of opening degree has little effect on the turning point of the outlet flow channel.

To better prevent cavitation damage to the valve, we appropriately increased the valve outlet pressure for the calculation. Figure 18 shows the stepwise increase of the valve outlet pressure from 0.205 MPa (the saturated vapor pressure of water at this temperature) to 0.7 MPa. It can be seen from the figure that when the valve outlet pressure gradually increases to 0.7 MPa, the cavitation at the valve seat and the outlet flow channel almost disappears, with only a tiny cavitation area remaining at the third-stage valve sleeve.

## 5. CONCLUSIONS

In this study, a new type of multi-layer sleeve regulating valve as used in nuclear power plant is chosen as the research object. The standard  $k-\epsilon$  turbulence model, mixture multiphase flow model, and the Zwart–Gerber–Belamri cavitation model were combined to carry out research on the internal flow characteristics of this new multi-layer sleeve regulating valve. In addition, a corresponding experiment was designed to verify the accuracy of the numerical simulations. The main conclusions are as follows:

The pressure and velocity variation trends of the fluid inside the regulating valve remain the same even when the opening degree of the valve changes. However, as the valve opening decreases from 100% to 25%, the fluid pressure drop borne by the first and second-stage sleeves gradually decreases, and the third-stage sleeve begins to play the main role in reducing the fluid pressure in the valve (fluid pressure drop changes from 2 MPa to nearly 8.5 MPa in this stage). At the same time, the velocity of the fluid at the first and second-stage sleeves decreases sharply by approximately 60 m/s, while that of the third-stage sleeve rises sharply by approximately 40 m/s.

When the valve is fully opened, the fluid pressure

changes and fluid velocities in each level of the valve sleeves are relatively uniform (each stage provides 2–3 MPa pressure drop with approximately 90 m/s fluid velocity). This helps prevent erosion of the valve by fluid in a state of high pressure fluctuating velocity.

There are three areas prone to cavitation inside the multi-layer sleeve regulating valve: the small hole near the wall of the third-stage sleeve, the small holes at the valve seat, and the turning point of the outlet flow channel. When decreasing the valve opening, the cavitation degree at the third-stage sleeve decreases, while that at the small holes at the valve seat increases correspondingly. The change of opening degree has little effect on the turning point of the outlet flow channel. To reduce the degree of cavitation, it is recommended to adjust the outlet pressure of the valve to 0.7 MPa (the saturated vapor pressure is 0.205 MPa) to prevent cavitation from the valve seat and the outlet flow channel. As for the cavitation at the sleeve, further work should be carried out to address structural optimization.

## ACKNOWLEDGMENTS

The work is supported by the National Key Research and Development Program of China (No. 2018YFB2004002), we are grateful for their support.

## REFERENCES

- Alqahtani, S., H. M. Ali, F. Farukh and K. Kandan (2023). Experimental and computational analysis of polymeric lattice structure for efficient building materials. *Applied Thermal Engineering* 218, 119366.
- Asim, T., M. Charlton and R. Mishra (2017). CFD based investigations for the design of severe service control valves used in energy systems. *Energy Conversion and Management* 153, 288-303.
- Chen, F. and Z. Jin (2021). Throttling components effect on aerodynamic performance of superheated steam flow in multi-stage high pressure reducing valve. *Energy* 230, 120769.
- Chen, F., J. Qian, M. Chen, M. Zhang, L. Chen and Z. Jin (2018). Turbulent compressible flow analysis on multi-stage high pressure reducing valve. *Flow Measurement and Instrumentation* 61, 26-37.
- Chen, F., M. Zhang, J. Qian, L. Chen and Z. Jin (2017). Pressure analysis on two-step high pressure reducing system for hydrogen fuel cell electric vehicle. *International Journal of Hydrogen Energy* 42(16), 11541-11552.
- Coşkun, G. and H. Pehlivan (2021). Fluid-structure interaction simulation of excess flow valve movement at different operating pressures and

- gas flow rates. *Journal of Applied Fluid Mechanics* 14(2), 615-625.
- Cui, B., Z. Lin, Z. Zhu, H. Wang and G. Ma (2017). Influence of opening and closing process of ball valve on external performance and internal flow characteristics. *Experimental Thermal and Fluid Science* 80, 193-202.
- Derakhshan, S., B. Beigzadeh, M. Rashidi and H. Pourrahmani (2019). Performance improvement and two-phase flow study of a piezoelectric micropump with tesla nozzle-diffuser microvalves. *Journal of Applied Fluid Mechanics* 12(2), 341-350.
- Echouchene, F., H. Belmabrouk, L. Le Penven and M. Buffat (2011). Numerical simulation of wall roughness effects in cavitating flow. *International Journal of Heat and Fluid Flow* 32(5), 1068-1075.
- Geng, K., C. Hu, C. Yang and R. Rong (2021). Numerical investigation on transient aerothermal characteristics of a labyrinth regulating valve for nuclear power plant. *Nuclear Engineering and Design* 382, 111369.
- Ma, Y., M. Zhang and H. Luo (2020). *Numerical And Experimental Studies of Gas-Liquid Flow and Pressure Drop in Multiphase Pump Valves*. Science Progress.
- Ou, G., X. Cao, C. Wang, A. Duan and H. Jin (2022). Cfd-dem-based numerical simulation of erosion characteristic of multistage pressure relief string regulating valve. *Journal of Applied Fluid Mechanics* 15(4), 999-1015.
- Qian, J., C. Hou, J. Mu, Z. Gao and Z. Jin (2020). Valve core shapes analysis on flux through control valves in nuclear power plants. *Nuclear Engineering and Technology* 52(10), 2173-2182.
- Qiu, C., C. Jiang, H. Zhang, J. Wu and Z. Jin (2019). Pressure drop and cavitation analysis on sleeve regulating valve. *Processes* 7(11).
- Shahsavari, A., A. H. A. Alwaeli, N. Azimi, S. Rostami, K. Sopian, M. Arıcı, P. Estellé, S. Nižetić, A. Kasaeian, H. M. Ali, Z. Ma and M. Afrand (2022). Exergy studies in water-based and nanofluid-based photovoltaic/thermal collectors: Status and prospects. *Renewable and Sustainable Energy Reviews* 168, 112740.
- Siddiqi, H. R., A. Qamar, R. Shaikat, Z. Anwar, M. Amjad, M. Farooq, M. M. Abbas, S. Imran, H. Ali, T. M. Y. Khan, F. Noor, H. M. Ali, M. A. Kalam and M. E. M. Soudagar (2022). Heat transfer and pressure drop characteristics of ZnO/DIW based nanofluids in small diameter compact channels: An experimental study. *Case Studies in Thermal Engineering* 39, 102441.
- Xavier, T. C. L. and J. P. Ortiz (2021). Three-dimensional simulations and economical solutions for cavitation in hollow-jet dispersive valves. *Journal of Applied Fluid Mechanics* 14(5), 1399-1410.
- Xu, X., L. Fang, A. Li, Z. Wang and S. Li (2021). Numerical analysis of the energy loss mechanism in cavitation flow of a control valve. *International Journal of Heat and Mass Transfer* 174, 121331.
- Yang, L., Z. Wang, W. Dempster, X. Yu and S. T. Tu (2017). Experiments and transient simulation on spring-loaded pressure relief valve under high temperature and high pressure steam conditions. *Journal of Loss Prevention in the Process Industries* 45, 133-146.
- Yi, D., L. Lu, J. Zou and X. Fu (2015). Interactions between poppet vibration and cavitation in relief valve. *Proceedings of the Institution of Mechanical Engineers, Part C: Journal of Mechanical Engineering Science* 229(8), 1447-1461.
- Yu, L., W. Chen, Z. Jin, C. Qiu and J. Qian (2022). Effect of sleeve orifices ratio on flow performance and hydrodynamic noise in the two-stage sleeve control valve. *Proceedings of the Institution of Mechanical Engineers, Part C: Journal of Mechanical Engineering Science*.
- Yuan, W., J. Sauer and G. H. Schnerr (2001). Modeling and computation of unsteady cavitation flows in injection nozzles. *Mécanique & Industries* 2(5), 383-394.
- Zawawi, N. N. M., W. H. Azmi, A. A. M. Redhwan, A. I. Ramadhan and H. M. Ali (2022). Optimization of air conditioning performance with al<sub>2</sub>o<sub>3</sub>-sio<sub>2</sub>/pag composite nanolubricants using the response surface method. *Lubricants* 10(10), 243.
- Zeng, L., G. Liu, J. Mao, S. Wang, Q. Yuan, H. Yuan, K. Wang, J. Zhang and Y. Xu (2015). Flow-induced vibration and noise in control valve. *Proceedings of the Institution of Mechanical Engineers, Part C: Journal of Mechanical Engineering Science* 229(18), 3368-3377.
- Zhang, Y., X. Liu, B. Li, S. Sun, J. Peng, W. Liu, J. He and W. Li (2022). Hydrodynamic characteristics and optimization design of a bio-inspired anti-erosion structure for a regulating valve core. *Flow Measurement and Instrumentation* 85, 102173.